THE ASTROPHYSICAL JOURNAL, 549:745–758, 2001 March 10


# THE STAR FORMATION HISTORY OF THE UNIVERSE: AN INFRARED PERSPECTIVE

MICHAEL ROWAN-ROBINSON
Astrophysics Group, Blackett Laboratory, Imperial College of Science Technology and Medicine, Prince Consort Road, London SW7 2BZ, England
*Received 2000 July 7; accepted 2000 November 14*

## ABSTRACT

A simple and versatile parameterized approach to star formation history allows a quantitative investigation of constraints from far-infrared and submillimeter counts and background intensity measurements. The models include four spectral components: infrared cirrus (emission from interstellar dust), an M82-like starburst, an Arp 220–like starburst, and an active galactic nucleus (AGN) dust torus. The 60 $\mu$m luminosity function is determined for each chosen rate of evolution using the Point Source Catalog Redshift Survey (PSC$z$) redshift data for 15,000 galaxies. The proportions of each spectral type as a function of 60 $\mu$m luminosity are chosen for consistency with *IRAS* and SCUBA color-luminosity relations, and with the fraction of AGNs as a function of luminosity found in 12 $\mu$m samples. The luminosity function for each component at any wavelength can then be calculated from the assumed spectral energy distributions (SEDs). With assumptions about the optical SEDs corresponding to each component and, for the AGN component, an assumed dependence of the dust covering factor on luminosity, the optical and near-infrared counts can be accurately modeled. High- and low-mass stars are treated separately, since the former will trace the rate of star formation, while the latter trace the cumulative integral of the star formation rate. A good fit to the observed counts at 0.44, 2.2, 15, 60, 90, 175, and 850 $\mu$m can be found with pure luminosity evolution in all three cosmological models investigated: $\Omega_0 = 1$, $\Omega_0 = 0.3$ ($\Lambda = 0$), and $\Omega_0 = 0.3$, $\Lambda = 0.7$. All three models also give an acceptable fit to the integrated background spectrum. Selected predictions of the models, for example redshift distributions for each component at selected wavelengths and fluxes, are shown. The effect of including an element of density evolution is also investigated. The total mass-density of stars generated is consistent with that observed, in all three cosmological models.

*Subject headings:* cosmology: observations — galaxies: evolution — galaxies: starburst — infrared: galaxies — stars: formation

## 1. INTRODUCTION

In this paper I investigate what source counts and the background radiation at infrared and submillimeter wavelengths can tell us about the star formation history of the universe. Madau et al. (1996) showed how the ultraviolet surveys of Lilly et al. (1996) could be combined with information on UV dropout galaxies in the Hubble Deep Field to give an estimate of the star formation history from $z = 0$ to 4 (see also Madau, Pozzetti, & Dickinson 1998). However these studies ignored what is already well known from far-infrared wavelengths, that dust plays a major role in redistributing the energy radiated at visible and UV wavelengths to the far infrared.

Subsequent to the Madau et al. analysis, several groups of authors have argued that the role of dust is crucial in estimates of the star formation rates at high redshifts. Rowan-Robinson et al. (1997) derived a surprisingly high rate of star formation at $z = 0.5$–1 from an *ISO* survey of the Hubble Deep Field (HDF). Subsequent *ISO* estimates by Flores et al. (1999) appear to confirm the need to correct for the effects of dust in estimates of star formation rates.

Large extinction-correction factors (5–10) were derived at $z = 2$–5 by Meurer et al. (1997, 1999). Pettini et al. (1998), Dickinson (1998), and Steidel et al. (1999) found that estimates of star formation rates derived from the HDF and other Lyman drop-out studies do indeed need to be corrected upward by a substantial factor (2–7). Thus, the high star formation rates deduced from the *ISO* HDF data (Rowan-Robinson et al. 1997) are not as out of line as at first appeared.

Many authors have attempted to model the star formation history of the universe ab initio (e.g., Kauffmann, White, & Guiderdoni 1993; Cole et al. 1994; Pei & Fall 1995; Baugh et al. 1998; Blain et al. 1999a; Somerville, Primack, & Faber 2000; Kauffmann & Haehnelt 2000). There is an even longer history of attempts to find empirical models for the evolution of the starburst galaxy population (e.g., Franceschini et al. 1991, 1994, 1997; Blain & Longair 1993; Pearson & Rowan-Robinson 1996; Guiderdoni et al. 1997, 1998; Dwek et al. 1998; Blain et al. 1999c; Dole et al. 2000). The study of Blain et al. (1999c) attempts a more systematic approach with a parameterized set of models but still treat the spectral energy distributions (SEDs) of the galaxies in a simplistic manner. In the present paper I report the results of a parameterized approach to the star formation history of the universe, which allows a large category of possible histories to be explored and quantified. The parametrized models can be compared with a wide range of source-count and background data at far-infrared and submillimeter wavelengths to narrow down the parameter space that the star formation history can occupy. The approach is similar to that of Guiderdoni et al. (1998) and Blain et al. (1999c), but differs in key respects outlined below.

An important development for understanding the role of dust in the star formation history of the universe has been the detection of the submillimeter background at wavelengths from 140 to 850 $\mu$m using *COBE* data (Puget et al. 1996; Schlegel, Finkbeiner, & Davis 1998; Hauser et al. 1998; Fixsen et al. 1998; Lagache et al. 1999). There is still

disagreement about the actual value of the background intensity by a factor of 2 at 850 $\mu$m and 2.5 at 140 $\mu$m.

Franceschini et al. (1997), Guiderdoni et al. (1998), Blain et al. (1999c), Dwek et al. (1998), and Gispert, Lagache, & Puget (2000) have presented models to account for this background radiation. The models of Guiderdoni et al. are able to account for the 350 and 850 $\mu$m background, but fail to fit the observed background at 140 and 240 $\mu$m, even if the lower values of Fixsen et al. are adopted. The models of Franceschini et al. (1997) invoke a new population of heavily obscured high-redshift starbursts, designed to account for the formation of spiral bulges and ellipticals. In this paper I test whether the submillimeter background and counts can be understood in terms of a single population of evolving star-forming galaxies. Blain et al. (1999c) put forward a range of models which they argue are consistent with all available counts and background radiation. I argue below that, among other problems, their most successful models involve an unphysical discontinuity in the star formation rate. Of the two most successful models of Dwek et al. (1998), one ("RR") is taken from an earlier version of the present work, and the other ("ED") involves a spike in the star formation history.

The layout of the paper is as follows. In § 2, I introduce a parameterized characterization of the star formation history that is both simple and versatile. Section 3 discusses the 60 $\mu$m luminosity function and evolution rate as derived from the *IRAS* Point Source Catalog Redshift Survey (PSC*z*). Section 4 discusses the assumed spectral energy distributions of galaxies as a function of luminosity, used to predict the luminosity functions at other wavelengths. Section 5 gives combined least-squares fits to the counts at 60 and 850 $\mu$m, and the background intensity at 140–750 $\mu$m in three selected cosmological models. Section 6 discusses the properties of the best-fitting models at a wide range of wavelengths. The effect of including some density evolution in an $\Omega_0 = 1$ model is discussed in § 7. Finally, § 8 gives discussion and conclusions. A Hubble constant of 100 km s$^{-1}$ Mpc$^{-1}$ is used throughout.

## 2. PARAMETRIZED APPROACH TO STAR FORMATION HISTORY

In this paper I present a parameterized approach to the problem, investigating a wide range of possible star formation histories for consistency with counts and background data from the ultraviolet to the submillimeter.

The constraints we have on the star formation rate, $\dot{\phi}_*(t)$, are that:

1. It is zero for $t = 0$.
2. It is finite at $t = t_0$.
3. It increases with $z$ out to at least $z = 1$ (and from condition 1, must eventually decrease at high $z$).

A simple mathematical form consistent with these constraints is

$$\frac{\dot{\phi}_*(t)}{\dot{\phi}_*(t_0)} = \exp Q\left(1 - \frac{t}{t_0}\right)\left(\frac{t}{t_0}\right)^P , \qquad (1)$$

where $P$ and $Q$ are parameters ($P > 0$ to satisfy condition 1, $Q > 0$ to satisfy condition 3). I assume that $\dot{\phi}_*(t) = 0$ for $z > 10$.

Equation (1) provides a simple but versatile parameterization of the star formation history, capable of reproducing most physically realistic, single-population scenarios. Figure 1 shows models of the type of equation (1) chosen to mimic the Pei & Fall (1995) models based on analysis of the history of heavy element formation, and also the Cole et al. (1994) semianalytic simulations of the star formation history in a cold dark matter (CDM) scenario (model *a*); those chosen to be consistent with the strong evolution rate seen by Lilly et al. (1996) in the Canada-France Redshift Survey (CFRS) (model *b*); and those fitted to far-infrared and submillimeter source counts and background intensity in different cosmological models (model *c*; for details see below). Models of the form of equation (1) will not, however, be able to reproduce the very sharply peaked scenario (ED) of Dwek et al. (1998), or the two-population model of Franceschini et al. (1997, 1998). In the scenarios modeled by equation (1), the formation of bulges and ellipticals are part of an evolving spectrum of star formation rates.

The physical meaning of the parameters is as follows. The exponential term describes an exponential decay in the star formation rate on a timescale $t_0/Q$, which can be interpreted as a product of the process of exhaustion of available gas for star formation (a competition between formation into stars and the return of gas to the interstellar medium from stars) and of the declining rate of galaxy interactions and mergers at later epochs. This parameter is the same as that used in the galaxy SED models of Bruzual & Charlot (1993). The power-law term represents the buildup of the rate of star formation due to mergers of fragments, which are incorporated into galaxies. The parameter $P$ measures how steeply

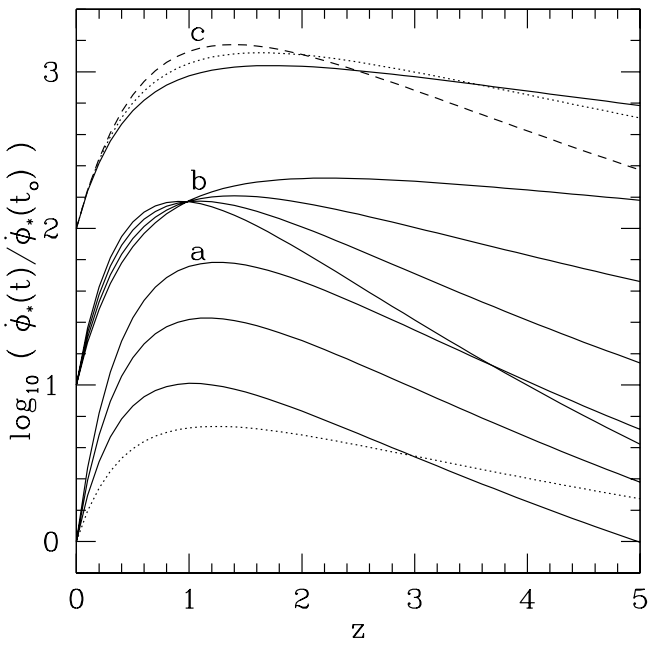


FIG. 1.—Examples of star formation histories of the form given in eq. (1): (*a*) Fitted to those predicted by Pei & Fall (1995); from the top, ($P$, $Q$) = (2.83, 8.15), (3.23, 10.25), (3.52, 11.92) from an infall model (their Figs. 1*d*, 3*d*, and 4*d*), using dereddened quasar Ly$\alpha$ absorber data, and (dotted curve) the prediction by Cole et al. (1994) derived from a CDM scenario, ($P$, $Q$) = (1.5, 5). (*b*) For $\Omega_0 = 1$ models consistent with Lilly et al. (1996) CFRS data, defined to have $\dot{\phi}_*(1)/\dot{\phi}_*(0) = 2^{3.9}$. From top at high $z$: ($P$, $Q$) = (1, 5.8), (2, 7.4), (3, 9.0), (5, 12.2). (*c*) Best-fit models for far-infrared and submillimeter counts and background for $\Omega_0 = 1$ [*solid curve*, ($P$, $Q$) = (1.2, 5.4)]; $\Omega_0 = 0.3$ [*dotted curve*, ($P$, $Q$) = (2.1, 7.3)]; $\Lambda = 0.7$ [*dashed curve*, ($P$, $Q$) = (3.0, 9.0)]. The curves for (*b*) and (*c*) have been displaced upward by +1 and +2, respectively.

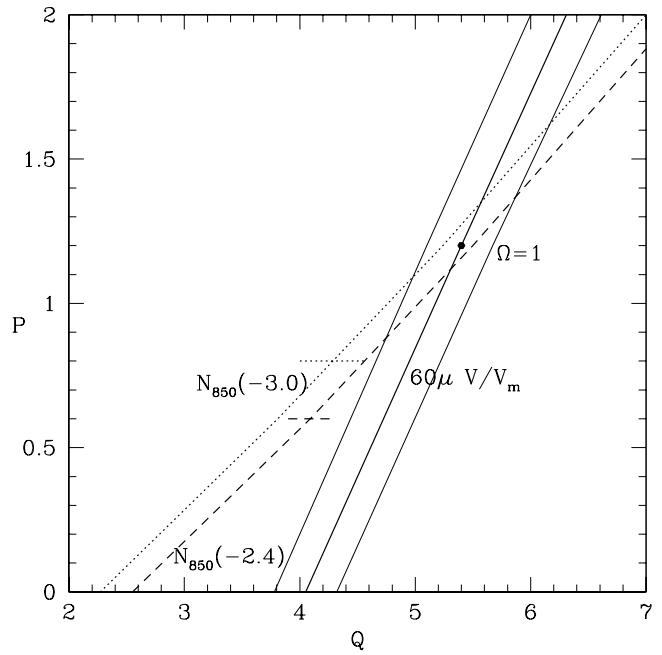


FIG. 2.—*P*-*Q* diagram, with loci for models fitting 60 $\mu$m counts and $V/V_m$ test (*solid curves*) and 850 $\mu$m counts (*dotted and dashed curves*). Counts loci correspond to $\log N_{850}(4\ \mathrm{mJy}) = 2.95 \pm 0.15$ (Hughes et al. 1998), and $\log N_{850}(1\ \mathrm{mJy}) = 3.90 \pm 0.15$ (Blain et al. 1999b). The locus corresponding to $\lg N_{60}(50\ \mathrm{mJy}) = 1.30$ (Hacking & Houck 1987) is almost identical to the 60 $\mu$m locus, with a slightly wider uncertainty ($\pm 0.28$ in $Q$).

this process occurs with time. The ratio $P/Q$ determines the location of the peak in the star formation rate, $t_{\mathrm{peak}}$, since $t_{\mathrm{peak}}/t_0 = P/Q$.

A very important assumption in the present work is that the star formation rate should vary smoothly with epoch. Several earlier models have assumed, for mathematical convenience, a discontinuous changes of slope in the star formation rate (e.g., Pearson & Rowan-Robinson 1996; the Blain et al. 1999c "anvil" models). Such discontinuities are highly unphysical, and I have eliminated them in this work. The assumption above that $\dot{\phi}_*(t) = 0$ for $z > 10$ represents just such an unphysical discontinuity in equation (1), and I have investigated the effect of replacing the power-law term in equation (1) by

$$(t/t_0)^P - (t_i/t_0)^P ,$$

where $t_i$ is the epoch at which star formation commences. This would then constitute a third parameter in the models, but one that has very little effect on the results, provided that $P > 1$, $z(t_i) \gg 1$. The Blain et al. (1999c) "peak 4" and "peak 5" models assume that there is no star formation at $z < 4$ and 5, respectively, and this constitutes a strong discontinuity within the observable range of redshifts, and so would again not be consistent with the philosophy adopted here. The Blain et al. (1999c) "peak 10" model is reasonable well approximated by $(P, Q) = (1.9, 10.15)$.

We might expect that the cosmological model could have a significant effect on the relationship between predicted counts and predicted background intensity, since the latter is sensitive to how the volume element and look-back time change with redshift.

To test this I have explored models with (1) $\Lambda = 0$, for which all the required formulae are analytic (specifically, here models with $\Omega_0 = 1$ and 0.3), and (2) $k = 0$, for which some of them are analytic (specifically, $\Lambda = 0.7$, $\Omega_0 = 0.3$). Relevant formulae are given in the Appendix.

## 3. 60 $\mu$m LUMINOSITY FUNCTION AND EVOLUTION DERIVED FROM *IRAS* PSC*z* SURVEY

Given an assumed $(P, Q)$, I then determine the 60 $\mu$m luminosity function using the *IRAS* PSC*z* sample (Saunders et al. 2000). I fit this with the form assumed by Saunders et al. (1990),

$$\eta(L) = C_*(L/L_*)^{1-\alpha} e^{-0.5[\log_{10}(1+L/L_*)/\sigma]^2} , \qquad (2)$$

and find that the luminosity function parameters can be well approximated as follows:

for $\Omega_0 = 1$:

$$\sigma = 0.744\text{–}0.033W ,$$
$$\log_{10} L_* = 8.50 + 0.05W - 2\log_{10}(H_0/100) ,$$
$$\text{where } W = Q - 1.125P ;$$

for $\Omega_0 = 0.3$ ($\Lambda = 0$):

$$\sigma = 0.748 - 0.028W ,$$
$$\log_{10} L_* = 8.46 + 0.05W - 2\log_{10}(H_0/100) ,$$
$$\text{where } W = Q - 1.10P ;$$

for $\Lambda = 0.7$ ($k = 0$):

$$\sigma = 0.783 - 0.030W ,$$
$$\log_{10} L_* = 8.39 + 0.05W - 2\log_{10}(H_0/100) ,$$
$$\text{where } W = Q - 1.067P .$$

I have assumed fixed values of $\alpha = 1.09$, $C_* = 0.027 (H_0/100)^3$. It is not clear that any previous studies have correctly taken into account the need to change the 60 $\mu$m luminosity function as the rate of evolution is varied. The study of Guiderdoni et al. (1998) explicitly violates the known constraints on the 60 $\mu$m luminosity function at the high-luminosity end, and as a result the models predict far too many high-redshift galaxies at a flux limit of 0.2 Jy at 60 $\mu$m, where substantial redshift surveys have already taken place. Blain et al. (1999c) state that they have determined the luminosity function from consistency with the 60 $\mu$m counts, but this process does not automatically give detailed consistency with existing redshift surveys.

We can also use the PSC*z* data to determine a range of consistency for $(P, Q)$, using the $V/V_m$ test. The predicted uncertainty in $\langle V/V_m \rangle$ for a population of $n$ galaxies, $(12n)^{-1/2}$, can be used to assign a goodness of fit for each set of $(P, Q)$ values. Figure 2 shows the locus of the best-fitting models in the $P$-$Q$ plane (for which $\langle V/V_m \rangle = 0.5$), together with the $\pm 1\,\sigma$ region, for $\Omega_0 = 1$.

## 4. ASSUMED INFRARED AND SUBMILLIMETER SPECTRAL ENERGY DISTRIBUTIONS

To transform this 60 $\mu$m luminosity function to other wavelengths, we must make an assumption about the spectral energy distributions. I have explored a variety of assumptions about these SEDs: (1) a single SED at all luminosities representative of starbursts; (2) composite SEDs that are a mixture of four components: a starburst component, a "cirrus" component, an Arp 220–like starburst,

and an active galactic nucleus (AGN) dust torus (cf. Rowan-Robinson & Crawford 1989; Rowan-Robinson & Eftstathiou 1993; Rowan-Robinson 1995), with the proportions of each depending on 60 $\mu$m luminosity (Rowan-Robinson 1999a, 1999b). Neither of these approaches gave satisfactory results, and it was not possible to find a simultaneous fit to all the far-infrared and submillimeter counts and background spectrum in any cosmological model. Models with luminosity-dependent composite SEDs could be found that fit the far-infrared and submillimeter counts and 850 $\mu$m background, but they failed to account for the 140–350 $\mu$m background. Finally, I have derived counts and background spectrum separately for each of the four components and then summed.

Thus,

$$N_\nu(S_\nu) = \sum_{i=1}^{4} \int \eta_{60}(L_{60}) t_i(L_{60}) dL_{60} \int_0^{z(L_{60}, S_\nu, \nu)} (dV/dz) dz \ , \tag{3}$$

where $\lg L_\nu = \lg L_{60} + \lg (L_\nu/L_{60}) = 6.18 + \lg S_\nu + \lg (\nu/\nu_{60}) + 2 \lg D_{\rm lum}(z) + k(z, \nu) + \lg [\dot{\phi}_*(z)/\dot{\phi}_*(0)]$, $L_\nu$ and $L_{60}$ are in solar units, $S_\nu$ is in Jy, $D_{\rm lum}$ is in Jy, and the $k$-correction is $k(z, \nu) = \lg [L_\nu(\nu(1 + z))/L_\nu(\nu)]$.

For small $z$,

$$\frac{dN_\nu(S_\nu)}{\eta_{60}(L_{60})(L_{60}/S_\nu)^{3/2}} = \sum_i t_i(L_{60}) \left(\frac{L_\nu}{L_{60}}\right)_i^{3/2} \ . \tag{4}$$

This approach finally gave satisfactory fits to all available data. It also allows a correct determination of the redshift distribution of each type separately as a function of wavelength and flux density, and the proportion of each type contribution to the counts at any flux density or to the background.

I have used the latest predictions for infrared SEDs of these components by Efstathiou, Rowan-Robinson, & Siebenmorgen (2000), and added near-IR/optical/UV SEDs corresponding to an Sab galaxy (Yoshii & Takahara 1988) for the cirrus and an H II galaxy (Tol 1924−416; Calzetti & Kinney 1992) for the starburst component, respectively. The starburst model is a good fit to multiwavelength data for M82 and NGC 6092 (Efstathiou et al. 2000), and also to far-infrared and submillimeter data for luminous starbursts (Rigopoulou, Lawrence, & Rowan-Robinson 1996).

The normalization between far-infrared and optical-UV components is determined by $L(60\ \mu{\rm m})/L(0.8\ \mu{\rm m}) = 0.15$ for the cirrus component, 5.3 for the starburst component, and 49 for the Arp 200 component. For the AGN component, I assume that $L(10\ \mu{\rm m})/L(0.1\ \mu{\rm m}) = 0.3$ (cf. Rowan-Robinson 1995) for the most luminous AGN, and that this ratio increases with decreasing luminosity to account for the fact that the mean covering factor is higher at lower luminosities. Therefore, $\lg L(10\ \mu{\rm m})/L(0.1\ \mu{\rm m}) = -0.52 + 0.1*(14.0 - \log L_{60})$.

For the cirrus component I have, somewhat arbitrarily, divided the optical SED into a contribution of young, high-mass stars (dominating at $\lambda \leq 0.3\ \mu$m) and a contribution of old, low-mass stars (dominating at $\lambda \geq 0.3\ \mu$m; see Fig. 3). The former are assumed to trace the star formation rate, and so participate in the strong evolution of the form of equation (1), but the latter trace the cumulative star formation up to the epoch observed, effectively a negative evolution with increasing redshift. This treatment, although approximate, allows a reasonable prediction of the $K$- and $B$-band counts. The two components in Figure 3 can be modeled, assuming $L \propto M^3$, blackbody SEDs with $T \propto L^{1/2}$, and with a Salpeter mass function, with mass range of 0.1–1 $M_\odot$ for the low-mass star component and 8–40 $M_\odot$ for the high-mass star component.

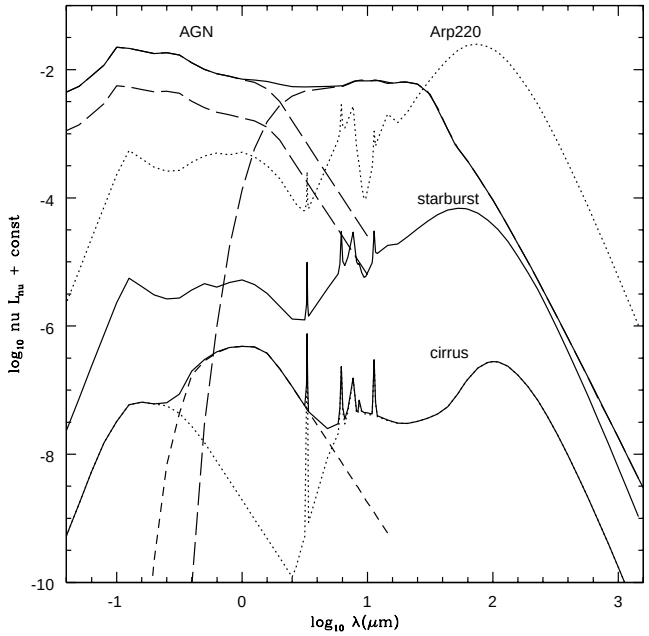


FIG. 3.—Adopted spectral energy distributions for the four components adopted in this study: cirrus (with optical emission split into low-mass [*dashed curve*], and high-mass [*dotted curve*] stars), M82 starburst, Arp 220 starburst (models from Efstathiou et al. 2000), and AGN dust torus (model from Rowan-Robinson 1995), showing assumed optical/IR ratio at $\log L_{60} = 14$ (*upper curve*) and 8.

The proportions of the four components (at 60 $\mu$m) as a function of luminosity (Table 1) have been chosen to give the correct mean relations in the $S(25\ \mu{\rm m})/S(12\ \mu{\rm m})$, $S(60\ \mu{\rm m})/S(25\ \mu{\rm m})$, $S(100\ \mu{\rm m})/S(60\ \mu{\rm m})$, and $S(60\ \mu{\rm m})/S(850\ \mu{\rm m})$ versus $L(60\ \mu{\rm m})$ diagrams (Figs. 4–6). Where predictions are being compared with *IRAS* 12 $\mu$m data or (later) with *ISO* 15 or 6.7 $\mu$m counts, I take into account the width of the relevant observation bands by filtering with a top-hat filter of appropriate half-width. (0.23, 0.26, and 0.16 at 6.7, 12, and 15 $\mu$m, respectively). Otherwise, observations were assumed to be monochromatic. The relative proportion of the 60 $\mu$m emission due to AGN dust tori as a function of $L(60\ \mu{\rm m})$ is derived from the luminosity functions given by Rush, Malkan, & Spinoglio (1993; see Fig. 7). The resulting mean SEDs as a function of $L(60\ \mu{\rm m})$ are shown in Figure 8. Luminosity functions at different wavelengths and the infra-

TABLE 1

PROPORTION OF DIFFERENT SED TYPES AT 60 $\mu$m, $t_i(L_{60})$, AS FUNCTION OF $L_{60}$

| $\lg_{10} (L_{60}/L_\odot)$ | Cirrus | M82 Starburst | A220 Starburst | AGN Dust Torus |
|---|---|---|---|---|
| 8.0..... | 0.99 | 0.001 | 0.5E−10 | 0.0091 |
| 9.0..... | 0.80 | 0.1988 | 0.5E−7 | 0.0012 |
| 10.0 ..... | 0.50 | 0.4999 | 0.5E−4 | 0.5E−4 |
| 11.0 ..... | 0.10 | 0.85 | 0.05 | 0.19E−4 |
| 12.0 ..... | 0.1E−3 | 0.75 | 0.25 | 0.25E−6 |
| 13.0 ..... | 0.1E−7 | 0.75 | 0.25 | 0.25E−8 |
| 14.0 ..... | 0.1E−12 | 0.75 | 0.25 | 0.25E−10 |

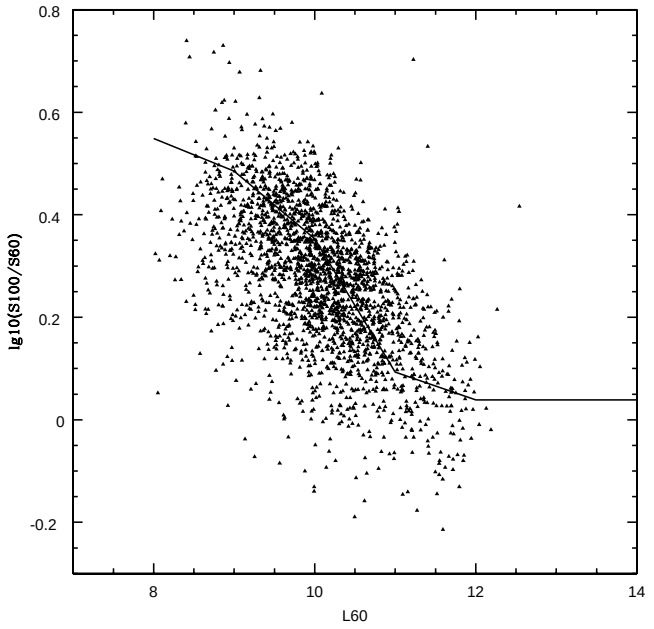


FIG. 4.—$S(100\ \mu m)/S(60\ \mu m)$ versus 60 $\mu$m luminosity for PSC$z$ galaxies. The solid line shows the trend with luminosity of the weighted average of the four component SEDs adopted.

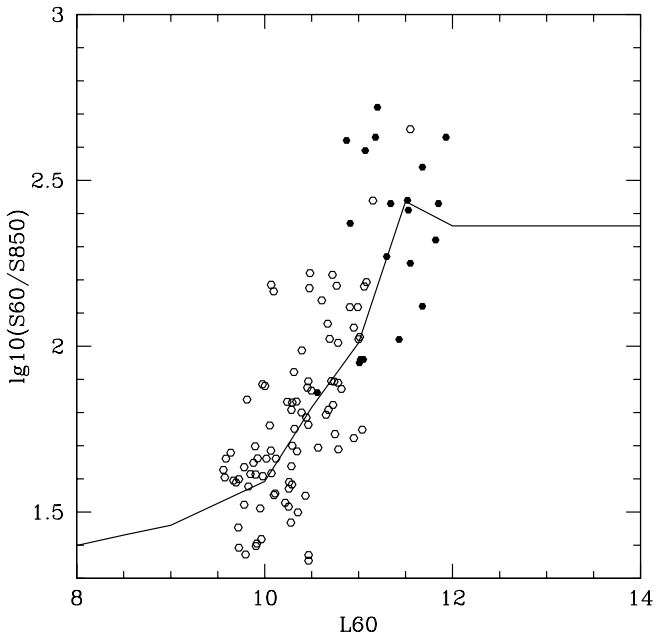


FIG. 6.—$S(60\ \mu m)/S(850\ \mu m)$ vs. 60 $\mu$m luminosity for galaxies observed by Rigopoulou et al. (1996), Dunne et al. (2000; *open circles*), and Fox et al. (2000).

red bolometric luminosity functions are shown in Figures 7 and 9–12. There is good agreement with measured luminosity functions at wavelengths from 0.44 to 850 $\mu$m. The agreement with the luminosity function derived at 60 $\mu$m from PSC$z$ data is unsurprising, since the luminosity function parameters were determined from these data. The fit to the 850 $\mu$m luminosity function of Dunne et al. (2000) is more impressive, since the transformation from 60 to 850 $\mu$m is based only on choosing the $t_i(L_{60})$ to give the correct ridgeline in Figure 6. The fit to the non-Seyfert data of Rush et al. (1993) at 12 $\mu$m is also impressive, again arising only from the choice of $t_i(L_{60})$ to be consistent with the color-luminosity diagrams in Figure 5. The fit to the Seyfert luminosity function at 12 $\mu$m is not fortuitous, since the $t_i(L_{60})$ for the AGN component were chosen to give this agreement. It is impressive that luminosity functions derived in the far-infrared can fit the data at 0.44 $\mu$m ($B$ band); the only freedom in the models to fit the $B$-band luminosity functions and counts is the amplitude of the optical SED relative to the far-infrared.

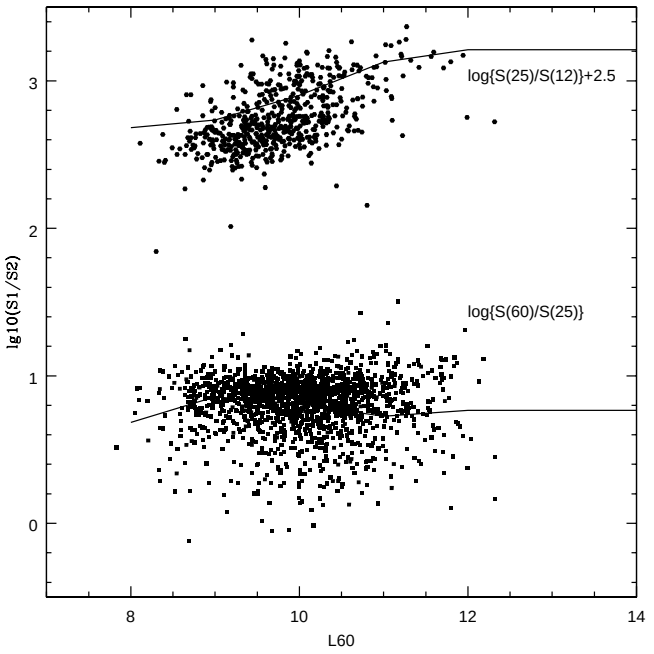


FIG. 5.—$S(25\ \mu m)/S(12\ \mu m)$ and $S(60\ \mu m)/S(25\ \mu m)$ versus 60 $\mu$m luminosity for PSC$z$ galaxies.

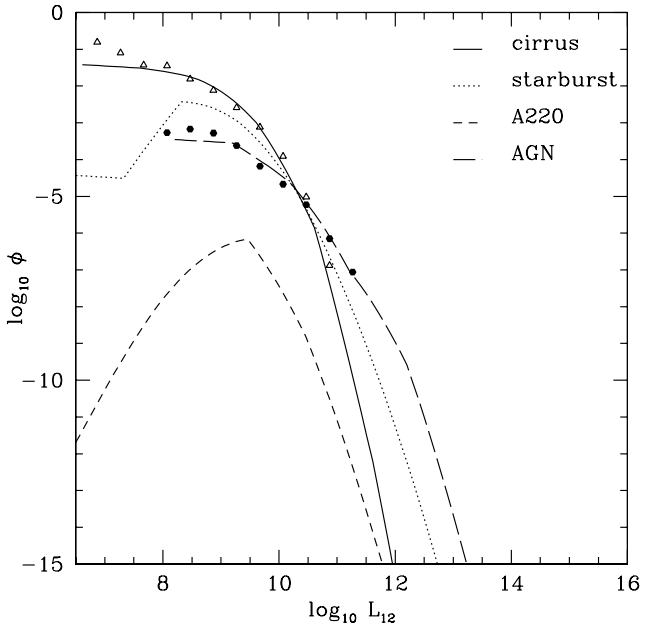


FIG. 7.—Luminosity functions at 12 $\mu$m for the four spectral components. Observed points taken from Rush et al. (1993) (*filled circles*: Seyfert galaxies; *open triangles*: non-Seyfert galaxies).

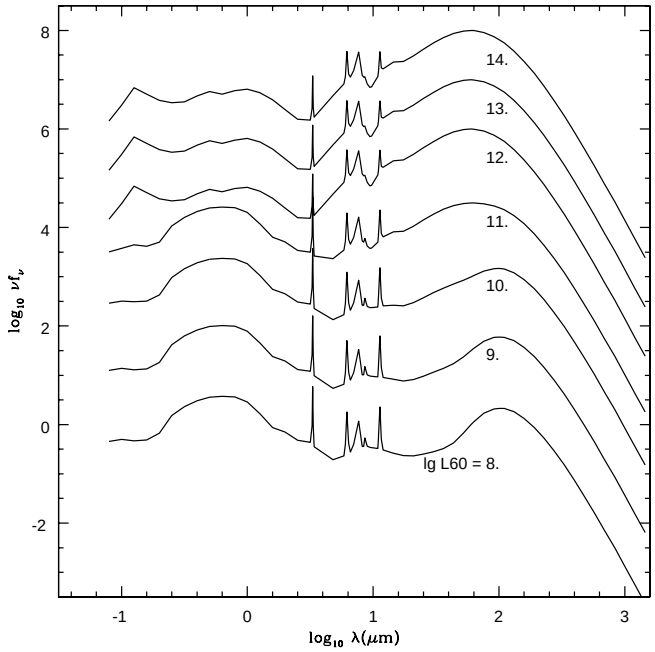


FIG. 8.—Average SED as a function of 60 $\mu$m luminosity, ranging from $\log_{10}(L_{60}/L_\odot) = 8$ to 14. The relative proportions of the different components, at 60 $\mu$m, are given in Table 1, and the average is calculated using eq. (4) (AGN dust torus component excluded).

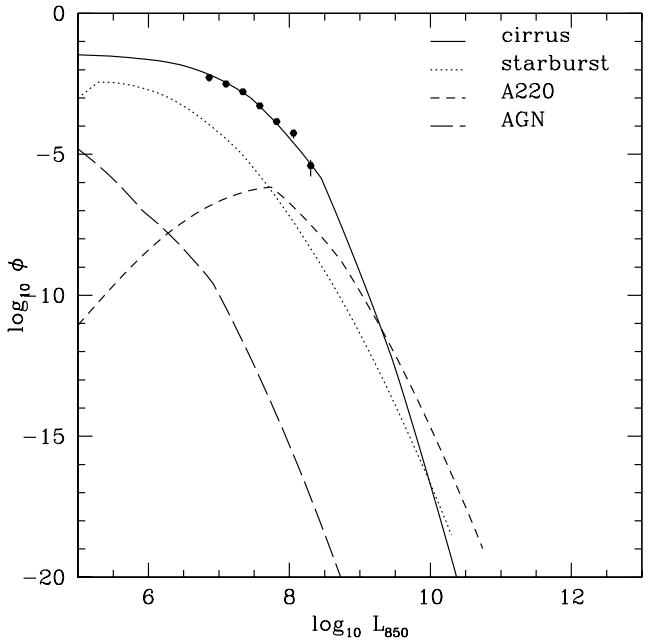


FIG. 10.—Luminosity functions at 850 $\mu$m for the four spectral components. The data are from Dunne et al. (2000).

Clearly, it will be important to have submillimeter data for a wide range of normal and active galaxies to test and improve these SEDs. However, the approach of using accurate radiative transfer models with realistic assumptions about dust grains, which have been verified with observations of known galaxies, seems superior to modeling the SED as a blackbody with power-law dust grain opacity in which the dust temperature is treated as a free parameter (as in Blain et al. 1999c). The latter approximation can only be valid for rest-frame wavelengths greater than 60 $\mu$m, i.e., for accurate prediction of counts and background intensities at wavelengths above 200 $\mu$m. Useful predictions can certainly not be made at 15 $\mu$m without explicit treatment of polycyclic aromatic hydrocarbons (PAHs). These criticisms do not apply to the studies of Guiderdoni et al. (1998), Dwek et al. (1998), Xu et al. (1998), and Dole et al. (2000), whose assumed SEDs are similar to those used here (but do not

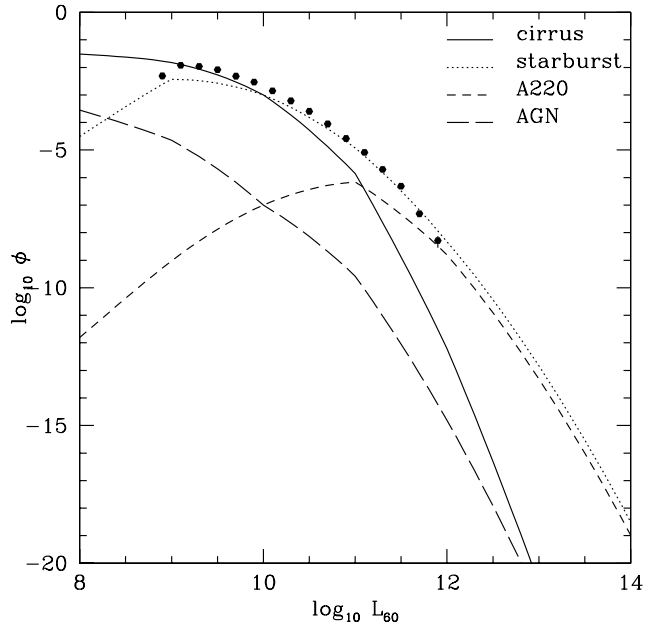


FIG. 9.—Luminosity functions at 60 $\mu$m for the four spectral components. Units of $\phi$ are Mpc$^{-3}$ dex$^{-1}$, luminosity ($\nu L_\nu$) in solar units. All luminosity functions are for a model with $\Omega_0 = 1$, $H_0 = 100$ km s$^{-1}$ Mpc$^{-1}$. Observed points are derived from PSC$z$ data.

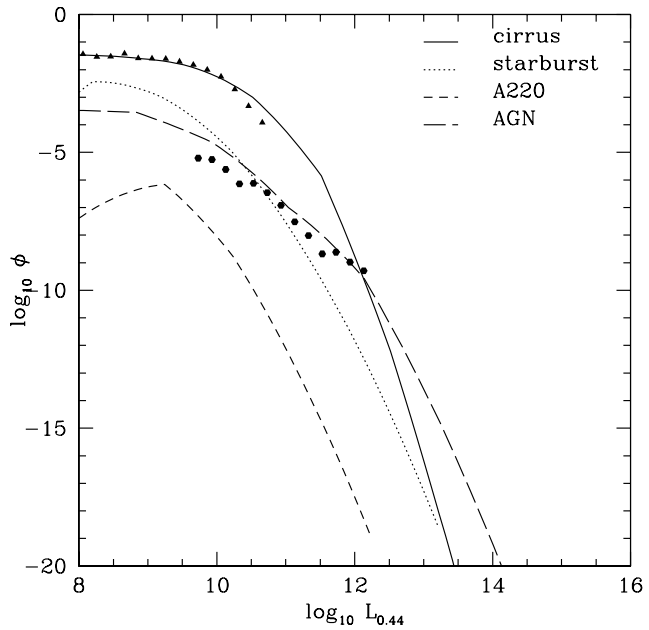


FIG. 11.—Luminosity functions at 0.44 $\mu$m for the four spectral components. Data for quasars derived from PG sample and for galaxies from Loveday et al. (1992).

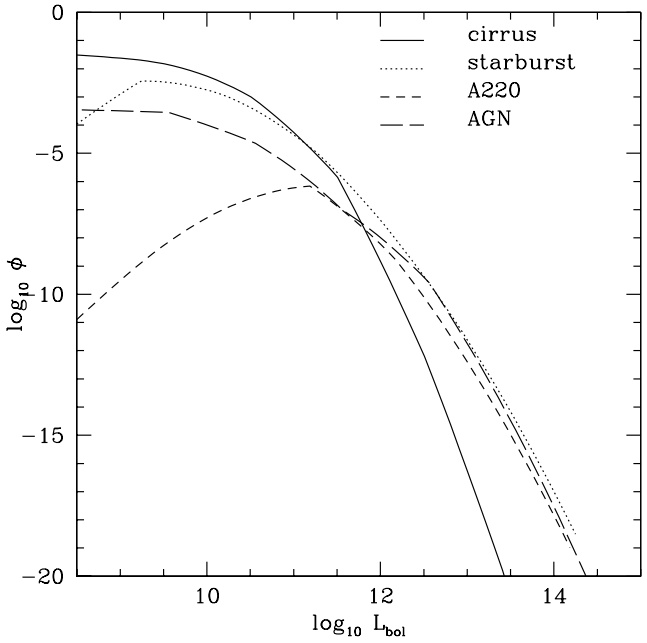


FIG. 12.—Bolometric luminosity functions for the four spectral components. Note that for luminosities greater than $10^{12.5}$ $L_{\odot}$ there is an approximately equal contribution from M82-type starbursts, Arp 220–like starbursts, and AGN dust tori.

include the detailed dependence on luminosity required for consistency with Figs. 4–6).

I have also assumed that the same luminosity evolution function should be applied to the whole 60 $\mu$m function, i.e., to AGN, "cirrus," and "starburst" components. I have investigated the effect of making the switchover in proportions of different types of components at a fixed luminosity, so that there is in effect a strong increase in the proportion of galaxies that are starbursts (or contain AGNs) with redshift. However, this did not permit a fit to all the available data, so I have assumed that the Table 1 proportions relate to the luminosity at zero redshift and that all these luminosities are subject to the evolution. This approach works, but models with more complex evolution than used here are clearly possible.

A substantial part of the illumination of the cirrus component in spiral galaxies is due to recently formed massive stars, part of whose light escapes directly from star-forming regions despite the high average optical depth in these regions. In the starburst models of Efstathiou et al. (2000), this corresponds to the late stages of their starburst models. If the typical starburst luminosity were greater in the past, then the emission from interstellar dust in the galaxy would also be correspondingly greater. However, the application of a uniform evolution rate to both the starburst and cirrus components of the far-infrared emission is not strictly self-consistent. At low redshifts the cirrus is illuminated by both low-mass and high-mass stars, with both contributing comparable energy inputs. At early epochs, the illumination will be predominantly from high-mass stars, since there would have been far fewer low-mass stars in the galaxy. Thus, the evolution of the cirrus component will be complex, depending on the star formation history, the evolution of metallicity, and the possibly varying dust geometry in the galaxy. The evolution of the SEDs of each component with redshift, particularly of the cirrus component, may be an important factor in understanding the counts and background, but is not treated here (see discussion in § 8).

It is possible that the evolution of AGNs differs from that of starburst at $z > 3$, but this will have little effect on the far-infrared counts and background (there could be a significant effect at 15 $\mu$m, which will be worth further study).

Elliptical galaxies are not treated explicitly, although their star formation rate must have been much greater in the past than at present. I am assuming that ellipticals are quiescent starburst galaxies, that their star formation proceeded in much the same way as we see in current live starbursts, and that their star formation episodes are part of the evolution history quantified here. We must think of this history as a series of short-lived fireworks taking place in different galaxies at different times. Similarly, this approach does not track the different spiral types separately, but only as a global average at each epoch.

## 5. COMBINED FITS TO 60, 175, AND 850 $\mu$m COUNTS, 140–750 $\mu$m BACKGROUND, AND DETERMINATION OF ($P$, $Q$)

I can now predict the counts and background intensity at any wavelength, and by comparing with observed values, constrain loci in the $P$-$Q$ plane. To determine ($P$, $Q$) for any given cosmological model, I combine the constraints found at 60 $\mu$m from the PSC$z$ (§ 4 above) with constraints from (1) deep counts at 60 $\mu$m (50 mJy), (2) the observed source counts at 850 $\mu$m at 1 and 4 mJy (see Table 2), and (3) the background intensity at 140, 350, and 750 $\mu$m. Figure 2 shows the constraints from the $V/V_m$ test and the 850 $\mu$m counts for the $\Omega_0 = 1$ case. The other constraints are less

TABLE 2

OBSERVED SOURCE COUNTS

| Wavelength ($\mu$m) | $\log_{10} S$(Jy) | $\log_{10} N(>S)$ | Reference |
|---|---|---|---|
| 15..... | −3.60 | $3.56 \pm 0.135$ | 1 |
| | −2.92 | $1.93 \pm 0.13$ | 2 |
| | −3.30 | $2.93 \pm 0.13$ | 2 |
| | −3.70 | $3.63 \pm 0.13$ | 2 |
| | −4.00 | $3.90 \pm 0.09$ | 2 |
| 60..... | 1.00 | −2.12 | 3 |
| | 0.5 | −1.39 | 3 |
| | 0.1 | −0.85 | 3 |
| | −0.22 | −0.38 | 4 |
| | −0.60 | $0.21 \pm 0.1$ | 3 |
| | −0.70 | 0.38 | 3 |
| | −1.00 | $0.76 \pm 0.07$ | 5 |
| | −1.30 | 1.46 | 6 |
| | −1.30 | $1.30 \pm 0.08$ | 5 |
| 175 ..... | −1.0 | $1.59 \pm 0.1$ | 7, 8 |
| 850 ..... | −2.40 | $2.95^{+0.15}_{-0.25}$ | 9 |
| | −2.70 | $3.40^{+0.15}_{-0.25}$ | 9 |
| | −2.55 | $3.25^{+0.13}_{-0.17}$ | 10 |
| | −2.40 | $3.39 \pm 0.19$ | 11 |
| | −2.65 | $3.37 \pm 0.30$ | 12 |
| | −3.00 | $3.90^{+0.14}_{-0.21}$ | 13 |
| | −2.155 | $2.56^{+0.23}_{-0.52}$ | 14 |

REFERENCES.—(1) Oliver et al. 1997; (2) Elbaz et al. 2000; (3) Lonsdale et al. 1990; (4) Rowan-Robinson et al. 1991; (5) Hacking & Houck 1987; (6) Kawara et al. 1998; (7) Gregorich et al. 1995; (8) Guiderdoni et al. 1998; (9) Hughes et al. 1998; (10) Eales et al. 1998; (11) Smail et al. 1997; (12) Barger et al. 1999; (13) Blain et al. 1999b; (14) Fox 2000.

TABLE 3

BEST-FIT STAR FORMATION HISTORY MODELS FOR $\Omega_0 = 1$, $\Omega_0 = 0.3$, AND $\Lambda = 0.7$

| Cosmological Model | $P$ | $Q$ | $l_{60}$ ($h\ L_\odot\ \mathrm{Mpc}^{-3}$) | $\xi$ | $\Omega_*$ ($h^{-1}$) |
|---|---|---|---|---|---|
| $\Omega_0 = 1$..... | 1.2 | 5.4 | 4.3 | 5.70 | 0.0027 |
| $\Omega_0 = 0.3$..... | 2.1 | 7.3 | 4.4 | 6.66 | 0.0032 |
| $\Lambda = 0.7$..... | 3.0 | 9.0 | 4.1 | 7.25 | 0.0033 |

important in specifying $P$ and $Q$. For all three cosmological models, values of $(P, Q)$ can be found that give a satisfactory fit to all the available data. As emphasized above, this outcome does depend strongly on the assumptions made about the SEDs.

An important constraint on the models is that the total mass of stars produced in galaxies should be consistent with the mass of stars observed, $\Omega_* = 0.003 \pm 0.0009\ h^{-1}$ (Lanzetta, Yahil, & Fernandez-Soto 1996), and that it should be less than the total density of baryons in the universe, $\Omega_* \leq \Omega_b = 0.0125 \pm 0.0025\ h^{-2}$ (Walker et al. 1991).

We can calculate the total mass density of stars from the 60 $\mu$m luminosity density using equation (7) of Rowan-Robinson et al. (1997), modified to take into account the latest Bruzual & Charlot galaxy evolution models (Madau et al. 1998; Rowan-Robinson 2000), from

$$\Omega_* = 10^{-11.13} \xi h^{-2} l_{60} (t_0/10\ \mathrm{Gyr})\ , \qquad (5)$$

where $l_{60}$ is the luminosity density in solar luminosities per $\mathrm{Mpc}^3$, $\xi = \int_0^1 [\dot{\phi}_*(t)/\dot{\phi}_*(t_0)] d(t/t_0)$, and the assumed fraction of optical-UV light being radiated in the far-infrared has been assumed to be $\epsilon = \frac{2}{3}$.

Table 3 gives the values of $(P, Q)$ that provide the best fit to the far-infrared and submillimeter counts and background for each of the three cosmological models considered, and the corresponding values of $l_{60}$, $\xi$, and $\Omega_*$, for an assumed age of the universe of $t_0 = 13$ Gyr. The predicted values of $\Omega_*$ are consistent with the observed value in each case. Estimating $\Omega_*$ from the young stellar component at 2800 Å or from the $K$-band luminosity density (with an assumed mass-to-light ratio) also give consistent results for an assumed Salpeter mass function.

## 6. PREDICTED COUNTS AND INTEGRATED BACKGROUND SPECTRUM FROM UV TO SUBMILLIMETER

Figures 13–19 show the predicted source counts in the three selected cosmological models at 850, 175, 90, 60, 15, 2.2, and 0.44 $\mu$m. The agreement with observations at infrared and submillimeter wavelengths is extremely impressive. Although the fits at 850 and 60 $\mu$m have been ensured by the least-squares procedure for determining $P$ and $Q$, the fits at 175, 90, and 15 $\mu$m are simply a consequence of the assumed SEDs and the choice of $t_i(L_{60})$. There is not much difference between the predictions of the three cosmological models at 60–850 $\mu$m. At 15 $\mu$m there is a difference between the models in the predicted number of sources at fluxes below 100 $\mu$Jy. The proportion of AGN dust tori at 12 $\mu$m agrees well that the data of Rush et al. (1993; 15% brighter than 0.4 Jy). Figure 17 shows that the proportion of AGNs at 15 $\mu$m is reasonably constant (15%–20%) for fluxes brighter than 3 mJy, but is predicted to fall rapidly toward fainter fluxes.

The fits to the counts at $B$ and $K$ are surprisingly good,

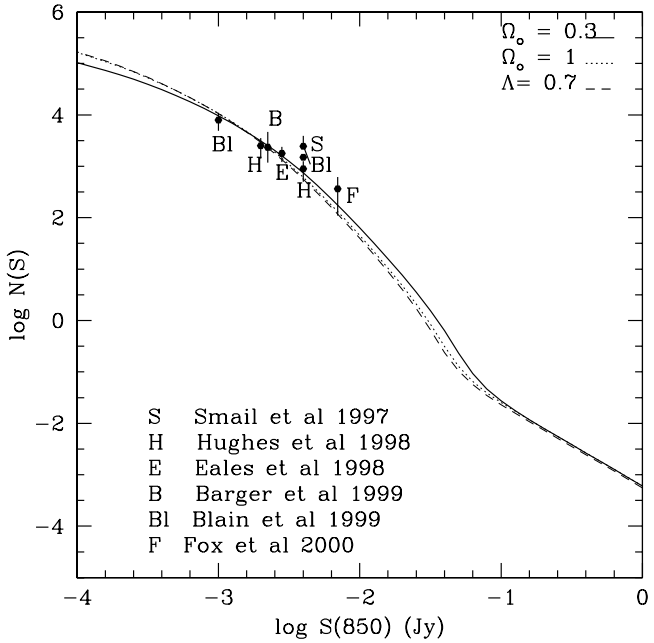


FIG. 13.—Integral source counts at 850 $\mu$m. Data are from Hughes et al. (1998), Eales et al. (1998), Smail, Ivison, & Blain (1997), Barger, Cowie, & Sanders (1999), Blain et al. (1999a), and Fox (2000). The three models shown are, from bottom at faint fluxes, for $\Omega_0 = 1$ and $(P, Q) = (1.2, 5.4)$ (*solid curve*); $\Omega_0 = 0.3$, $(P, Q) = (2.1, 7.3)$ (*dotted curve*); and $\Lambda = 0.7$, $(P, Q) = (3.0, 9.0)$ (*dashed curve*).

although the model does not at present have components capable of accounting for the very faint $K$- and $B$-band galaxy counts. This could be provided either by a measure of density evolution (see below) or by steepening the faint-end luminosity function at $z > 1$, which could in either case be attributed to a population of galaxies that had merged into present-day galaxies. The $B$-band galaxy counts are dominated by the (negatively evolving) low-mass star com-

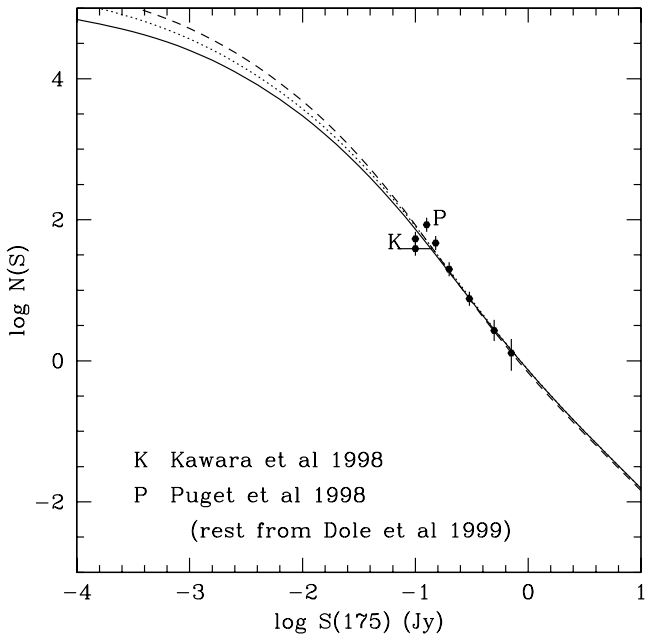


FIG. 14.—Source counts at 175 $\mu$m. Data points are from Kawara et al. (1998), Guiderdoni et al. (1998), and Dole et al. (2000). Models as in Fig. 13.

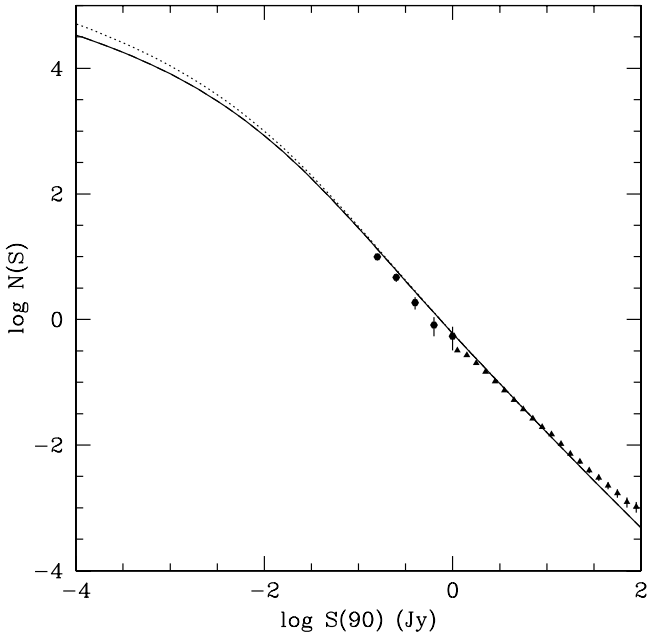


FIG. 15.—Source counts at 90 $\mu$m. Data from *IRAS* PSC*z* (*triangles*) and ELAIS (*filled circles*) are from Efstathiou et al. (2000). Models as in Fig. 13.

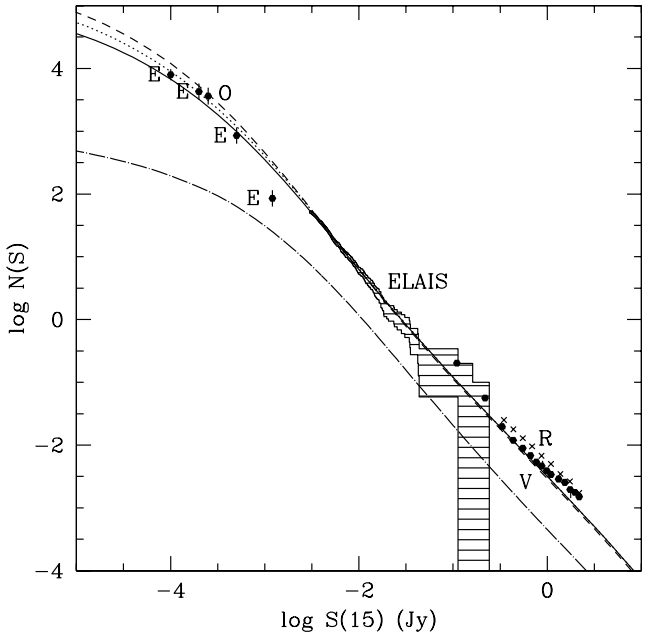


FIG. 17.—Source counts at 15 $\mu$m. Data from Oliver et al. (1997, "O"), Serjeant et al. (2000, "ELAIS"), Elbaz et al. et al. (2000, "E"), Rush et al. (1993, "R," *crosses*), and Verma (2000, "V," *filled circles*). Models as in Fig. 13. The lower dash-dotted line shows counts of the AGN dust torus population for the $\Omega_0 = 1$ model.

ponent for $\lg_{10} S(0.44\ \mu\text{m}) \geq -4.7$ Jy ($B_{AB} \leq 20.7$) and by the (positively evolving) high-mass star component at fainter fluxes. In the *I* band (0.8 $\mu$m), the crossover is at 23.7 m. The predicted median redshift for $I_{AB} \leq 22.5$ is 0.49, in good agreement with the results of the CFRS survey (Lilley et al. 1995), but for $B \leq 22$, the predicted median $z$ is 0.54, rather higher than the $\sim$0.3 observed by Colless et al. (1993), suggesting that we do not have quite the correct luminosity function or evolution for the blue galaxy population.

Figures 20–23 show redshift distributions at selected wavelengths and fluxes.[1] The median redshift at $S(850\mu\text{m}) \geq 2$ mJy (Fig. 20) is predicted to be 2.25, signifi-

[1] Complete output of the models is available at: http://astro.ac.uk/~mrr/countmodels.

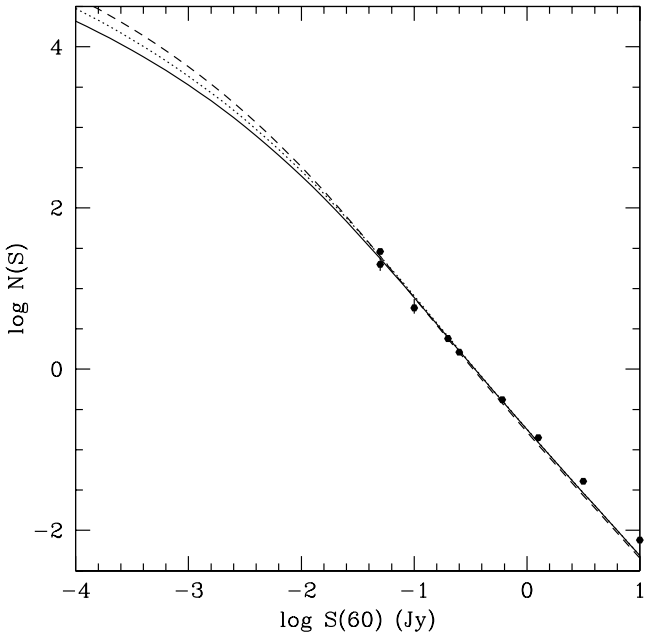


FIG. 16.—Source counts at 60 $\mu$m. Data are from Lonsdale et al. (1990) (at 0.2–10 Jy), Hacking & Houck (1987) (at 50–100 mJy), Rowan-Robinson et al. (1991), Gregorich et al. (1995) (higher point at 50 mJy; see Bertin, Dennefeld, & Moshir 1997 for discussion of possible contribution of cirrus to Gregorich et al. counts). Models as in Fig. 13.

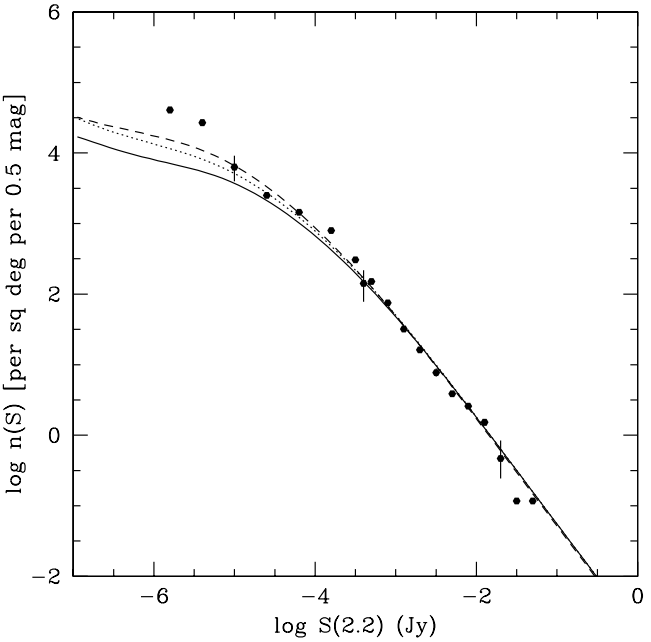


FIG. 18.—Differential source counts at 2.2 $\mu$m. Data from McCracken et al. (2000). Models as in Fig. 13.

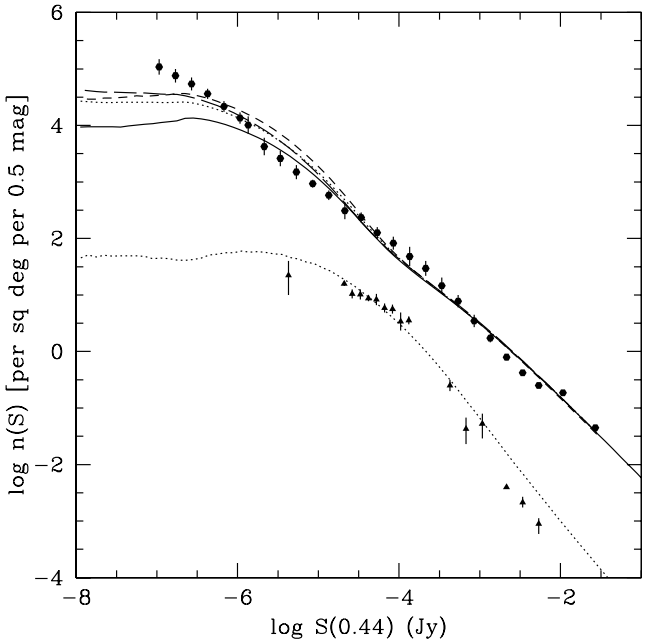


FIG. 19.—Differential source counts at 0.44 $\mu$m. Galaxy data are from Metcalfe et al. (1995), quasar data from Boyle, Shanks, & Peterson (1988). Models as in Fig. 13; Lower dotted curve is prediction for quasars in $\Omega_0 = 1$ model. The long-dashed line shows the effects of including density evolution (see text) on the $\Omega_0 = 1$ model.

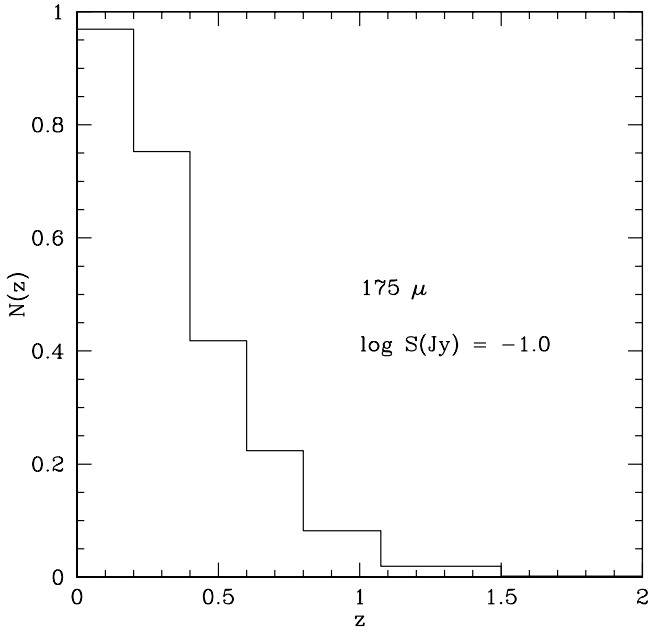


FIG. 21.—Predicted redshift distribution at 175 $\mu$m, $\log_{10} S(\mathrm{Jy}) = -1.0$.

cantly deeper than the prediction for $S(0.44\ \mu\mathrm{m}) \geq 0.1\ \mu$Jy ($B_{AB} \leq 26.4$ mag), 1.63 (Fig. 23). Only for $B_{AB} \leq 29$ do we reach the same predicted median $z$ as for 850 $\mu$m. This shows the power of the 850 $\mu$m surveys and also the difficulty there will be in identifying the sources detected.

Figure 24 shows the predicted integrated background spectrum for the three cosmological models compared with the submillimeter observations summarized in Table 4, the optical and near-infrared estimates of Pozzetti et al. (1998), and the 15 $\mu$m estimate of Sergeant et al. (2000). Dwek et al. (1998) have argued by extrapolation from longer wavelengths that the 100 $\mu$m background should lie in the range 5–34 nW m$^{-2}$ sr$^{-1}$, but since this is not a true measurement of the background I have not used it here (my models lie within the estimated range). Dwek & Arendt (1998), Gorjian, Wright, & Chang (2000), and Wright & Reese (2000) have given estimates of the background at 2.2 and 3.5

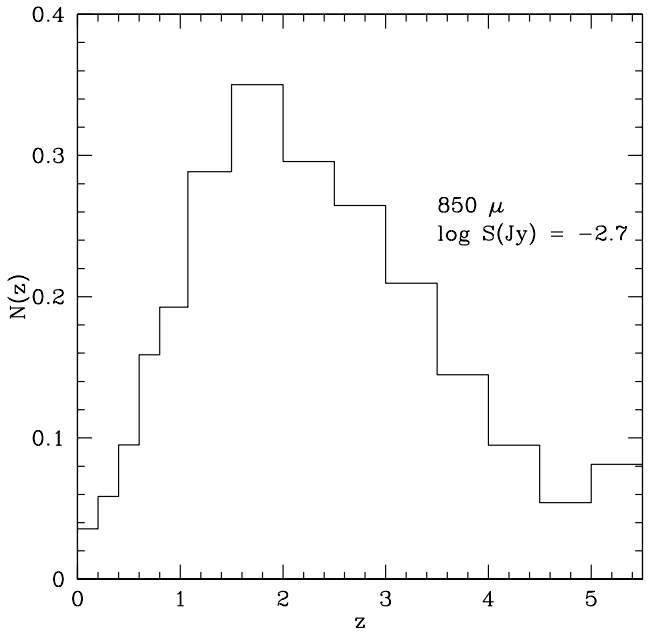


FIG. 20.—Predicted redshift distribution at 850 $\mu$m, $\log_{10} S(\mathrm{Jy}) = -2.7$. Bin centered at $z = 5.25$ refers to $z > 5$.

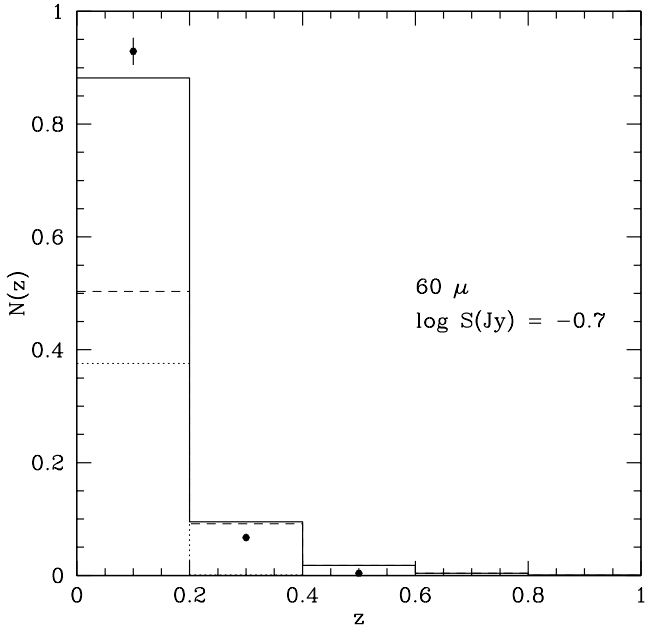


FIG. 22.—Predicted redshift distribution at 60 $\mu$m, $\log_{10} S(\mathrm{Jy}) = -0.7$. Contribution from cirrus is shown by dotted histogram, that from starbursts by dashed histogram. Observed points are derived from the FSS$z$ redshift survey of Oliver et al. (1996).

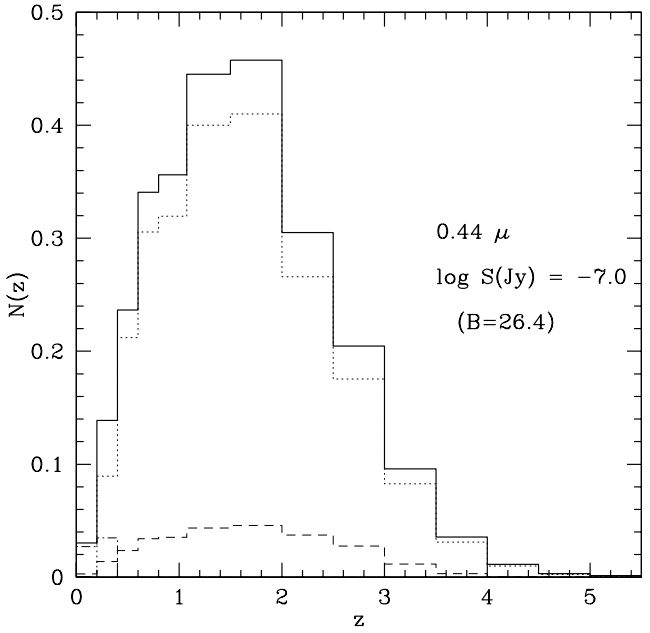


FIG. 23.—Predicted redshift distribution at 0.44 $\mu$m, $\log_{10} S(\mathrm{Jy}) = -7.0$ (corresponding to $B_{AB} = 26.4$). Dotted and dash-dotted curves show contributions of high- and low-mass stars; dashed curve shows contribution of starburst component.

TABLE 4

OBSERVED SUBMILLIMETER BACKGROUND

| Wavelength ($\mu$m) | $\log_{10} \nu I_\nu$ (nW m$^{-2}$ sr$^{-1}$) | Reference |
|---|---|---|
| 140 ..... | $1.51^{+0.14}_{-0.23}$ | 1 |
| | $1.40^{+0.11}_{-0.15}$ | 2 |
| | $1.10 \pm 0.10$ | 3 |
| | $1.18^{+0.15}_{-0.23}$ | 4 |
| 240 ..... | $1.00 \pm 0.20$ | 5 |
| | $1.23^{+0.09}_{-0.12}$ | 1 |
| | $1.15^{+0.08}_{-0.11}$ | 2 |
| | $1.04 \pm 0.10$ | 3 |
| | $1.06^{+0.06}_{-0.08}$ | 4 |
| 350 ..... | $0.85 \pm 0.20$ | 5 |
| | $0.78 \pm 0.10$ | 3 |
| | $0.85^{+0.13}_{-0.21}$ | 4 |
| 500 ..... | 0.37 | 3 |
| | $0.59^{+0.16}_{-0.26}$ | 4 |
| 750 ..... | −0.12 | 3 |
| | $-0.05^{+0.11}_{-0.14}$ | 4 |
| 850 ..... | $0.00 \pm 0.15$ | 5 |
| | $-0.30 \pm 0.10$ | 3 |

REFERENCES.—(1) Schlegel et al. 1998; (2) Hauser et al. 1998; (3) Fixsen et al. 1998; (4) Lagache et al. 1999; (5) Puget et al. 1996.

$\mu$m, which appear to be a factor 2 or more higher than estimates derived from summing deep galaxy counts (Pozzetti et al. 1998). This would seem to imply either incomplete subtraction of foreground emissions or some additional background unconnected with galaxies, and I have not used these estimates.

The models shown in Figure 24 are consistent with the observations, although the predictions of the $\Omega_0 = 1$ model are on the low side, while those of the $\Lambda = 0.7$ model are on the high side. Figure 25 shows, for the $\Omega_0 = 1$ model, the contribution of the different SED types to the background. The dominant contribution is from the cirrus component at most wavelengths, so the prediction is that more of the energy from starbursts is deposited in the general interstellar medium of a galaxy than is absorbed in the early stages close to the location of the massive stars. This dominance by the cirrus component at submillimeter wavelengths

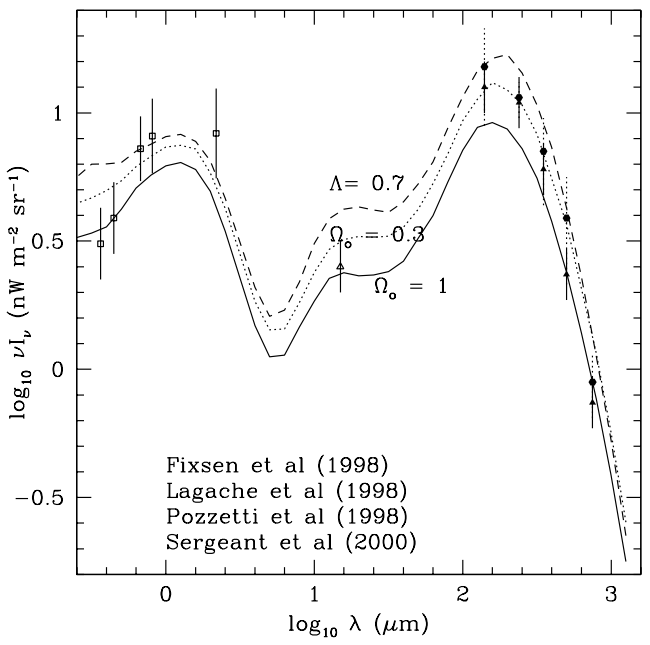


FIG. 24.—Predicted spectrum of integrated background for same models as in Fig. 10. Data from Fixsen et al. (1998) (far-IR and submillimeter), Pozzetti et al. (1998) (optical and UV), and Serjeant et al. (2000) (15 $\mu$m).

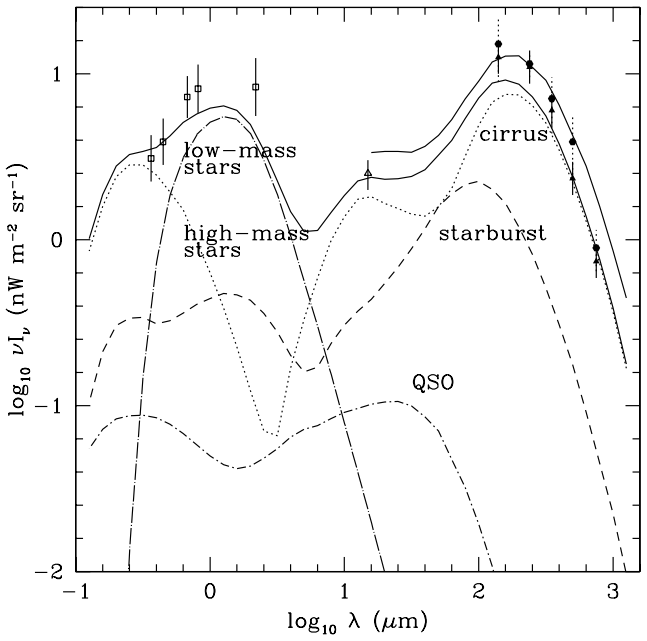


FIG. 25.—Predicted spectrum of integrated background for $\Omega_0 = 1$ model, showing contribution of the different components. The contribution of the Arp 220–like starbursts is less than 0.01 nW m$^{-2}$ at all wavelengths. The upper solid curve at long wavelengths shows the effect of including density evolution (see text).

TABLE 5

PREDICTED INTEGRATED BACKGROUND FLUX FROM DIFFERENT COMPONENTS, FOR $\Omega_0 = 1$, $\Omega_0 = 0.3$, AND $\Lambda = 0.7$

| | $\nu I_\nu$ (nW m$^{-2}$ sr$^{-1}$) | | | | | | | | | | | |
|---|---|---|---|---|---|---|---|---|---|---|---|---|
| | 0.1–5 $\mu$m | | | 5–100 $\mu$m | | | 100–1600 $\mu$m | | | Total | | |
| COMPONENT | $\Omega_0 = 1$ | $\Omega_0 = 0.3$ | $\Lambda = 0.7$ | $\Omega_0 = 1$ | $\Omega_0 = 0.3$ | $\Lambda = 0.7$ | $\Omega_0 = 1$ | $\Omega_0 = 0.3$ | $\Lambda = 0.7$ | $\Omega_0 = 1$ | $\Omega_0 = 0.3$ | $\Lambda = 0.7$ |
| Cirrus + Starlight ..... | 13.81 | 15.73 | 18.07 | 5.30 | 6.94 | 9.01 | 10.09 | 14.30 | 18.45 | 28.20 | 36.97 | 45.36 |
| M82 Starburst ..... | 1.25 | 1.71 | 2.11 | 2.68 | 3.56 | 4.35 | 1.83 | 2.63 | 3.25 | 5.76 | 7.90 | 9.71 |
| Arp 220 Starburst ..... | 0.0004 | 0.0006 | 0.0007 | 0.004 | 0.005 | 0.006 | 0.0074 | 0.0103 | 0.0122 | 0.0118 | 0.0159 | 0.0189 |
| AGN + Dust Torus..... | 0.243 | 0.320 | 0.432 | 0.247 | 0.333 | 0.431 | 0.0074 | 0.0106 | 0.0116 | 0.490 | 0.674 | 0.875 |
| Total (all types) ..... | 14.34 | 17.75 | 20.61 | 8.21 | 10.86 | 13.63 | 11.91 | 16.95 | 21.73 | 34.46 | 45.56 | 55.97 |

also implies that many of the detected sources should turn out to be rather extended (kiloparsec scales rather than the more compact scales expected for nuclear starbursts). Table 5 gives the contributions of the four components, and totals, to the background flux in the wavelength ranges 0.1–5, 5–100, and 100–1250 $\mu$m. The totals are somewhat lower than those given by Gispert et al. (2000), based on summing all claimed measurements of the background.

## 7. EFFECT OF INCLUDING DENSITY EVOLUTION

In the framework of hierarchical, bottom-up galaxy formation scenarios, such as those based on cold dark matter, we expect that galaxies form as the result of mergers between smaller fragments. Thus, we might expect to see a higher total density of galaxies as we look back toward the past. To test whether attributing part of the star formation history to density evolution has a major effect on the predicted counts and backgrounds, I have considered, for the $\Omega_0 = 1$ case, a simple modification in which the comoving density of galaxies varies with redshift as $\rho(z) = \rho(0)(1 + z)^n$.

For $n = 1$, this means that the comoving number density of galaxies at redshifts 2, 5, and 10 (our assumed cutoff redshift) is increased by a factor of 3, 6, and 11, respectively, compared to the present. This would represent a very substantial degree of merging of galaxies over the observable range of redshifts.

Since the background intensity depends on the product of the luminosity and density evolution rates, the background spectrum will be unaltered if we simply increase $P$ by $2n/3$. At low redshifts, the counts will be unaffected if $P$ is increased by $n/3$. I find that for a combined density evolution model with $n = 1$ and luminosity evolution with $P = 1.5$, $Q = 5.4$ (and $\Omega_0 = 1$), the fits to the counts at 15–850 $\mu$m hardly change over the observed range, but the predicted background is raised by about 0.2 dex, giving better agreement with observations for this cosmological model. For the $\Lambda = 0.7$ model, the fit to the background would be significantly worsened for models consistent with the observed counts.

## 8. PREDICTED CONFUSION-LIMITED PERFORMANCE OF INFRARED AND SUBMILLIMETER TELESCOPES

The source-count models derived here can be used to compare the ultimate performance of different infrared and submillimeter telescopes. To do this in a simple and transparent way, I treat confusion in a simplified but consistent

TABLE 6

CONFUSION LIMIT FOR DIFFERENT INFRARED AND SUBMILLIMETER TELESCOPES, FOR $\Omega_0 = 1$ MODEL

| | | | | | | REDSHIFT DISTRIBUTION (FRACTION) | | | | | |
|---|---|---|---|---|---|---|---|---|---|---|---|
| TELESCOPE | $D$ (m) | $\lambda$ ($\mu$m) | $2\theta_{conf}$ | $N_{conf}$ (per deg$^2$) | lg $S_{conf}$ (Jy) | 0–1 | 1–2 | 2–3 | 3–4 | 4–5 | >5 |
| *ISO* ..... | 0.6 | 15 | 6.″2 | 10800 | −4.22 | 0.7011 | 0.2858 | 0.0077 | 0.0009 | 0.0001 | 0.0 |
| | | 90 | 37.″1 | 300 | −1.66 | 0.9708 | 0.0290 | 0.0002 | 0.0 | 0.0 | 0.0 |
| | | 175 | 72.″2 | 79 | −0.97 | 0.9785 | 0.0212 | 0.0002 | 0.0 | 0.0 | 0.0 |
| SCUBA..... | 15. | 450 | 7.″4 | 590 | −1.90 | 0.3287 | 0.4850 | 0.1583 | 0.0258 | 0.0020 | 0.0002 |
| | | 850 | 14.″0 | 2100 | −2.63 | 0.1082 | 0.3193 | 0.2801 | 0.1772 | 0.0746 | 0.0406 |
| *SIRTF* ..... | 0.85 | 8.0 | 2.″33 | 75780 | −6.17 | 0.3829 | 0.4525 | 0.0868 | 0.0413 | 0.0172 | 0.0191 |
| | | 25 | 7.″3 | 7760 | −3.87 | 0.6062 | 0.3484 | 0.0428 | 0.0024 | 0.0001 | 0.0 |
| | | 70 | 20.″4 | 990 | −2.33 | 0.9314 | 0.0675 | 0.0010 | 0.0 | 0.0 | 0.0 |
| | | 160 | 46.″6 | 190 | −1.23 | 0.9741 | 0.0253 | 0.0003 | 0.0 | 0.0 | 0.0 |
| *Astro-F* ..... | 0.6 | 60 | 25″ | 700 | −2.36 | 0.9334 | 0.0655 | 0.0010 | 0.0 | 0.0 | 0.0 |
| | | 175 | 72.″2 | 79 | −0.97 | 0.9785 | 0.0212 | 0.0002 | 0.0 | 0.0 | 0.0 |
| *FIRST* ..... | 3.5 | 90 | 6.″4 | 10185 | −3.13 | 0.7456 | 0.2316 | 0.0211 | 0.0016 | 0.0001 | 0.0 |
| | | 120 | 8.″5 | 5730 | −2.50 | 0.8366 | 0.1546 | 0.0083 | 0.0004 | 0.0 | 0.0 |
| | | 175 | 12.″4 | 2680 | −1.96 | 0.8261 | 0.1683 | 0.0052 | 0.0003 | 0.0 | 0.0 |
| | | 250 | 17.″7 | 1320 | −1.73 | 0.7302 | 0.2609 | 0.0085 | 0.0004 | 0.0 | 0.0 |
| | | 350 | 24.″8 | 670 | −1.70 | 0.5469 | 0.4077 | 0.0432 | 0.0021 | 0.0001 | 0.0 |
| | | 500 | 35.″4 | 330 | −1.78 | 0.3454 | 0.4838 | 0.1469 | 0.0223 | 0.0016 | 0.0001 |
| | | 600 | 42.″5 | 230 | −1.88 | 0.2426 | 0.4805 | 0.2145 | 0.0544 | 0.0071 | 0.0010 |
| *Planck* ..... | (1.5) | 350 | 5′ | 4.6 | −0.83 | 0.8104 | 0.1851 | 0.0043 | 0.0001 | 0.0 | 0.0 |
| | | 550 | 5′ | 4.6 | −1.13 | 0.4454 | 0.4220 | 0.1222 | 0.0097 | 0.0005 | 0.0001 |
| | | 850 | 5′ | 4.6 | −1.63 | 0.1555 | 0.3732 | 0.3086 | 0.1310 | 0.0276 | 0.0040 |

manner. I assume that the 5 $\sigma$ confusion limit falls at a source density of 1 source per 40 beams, defined to be circular apertures of radius $\theta_{\rm conf} = 0.6\lambda/D$, where $D$ is the diameter of the telescope. The corresponding source-density limit is denoted $N_{\rm conf}$ per deg$^2$. The corresponding confusion limit and the fraction of sources in different redshift bins can then be estimated. The above assumption is valid for a population of sources with $N(S) \propto S^{-1.5}$ (Murdoch, Crawford, & Jauncey 1973; Condon 1974). The exact calculation depends slightly on the source-count slope.

Table 6 gives the wavelength, $2\theta_{\rm conf}$, $N_{\rm conf}$, $S_{\rm conf}$, and redshift distribution for my best $\Omega_0 = 1$ model, with $(P, Q) = (1.2, 5.4)$.

## 9. DISCUSSION AND CONCLUSIONS

I have developed a parameterized approach to the star formation history, which is sufficiently versatile to reproduce many proposed model histories. The model assumes that the evolution of the star formation rate manifests itself as pure luminosity evolution. I have stressed the importance of ensuring that the assumed luminosity function is consistent with available 60 $\mu$m redshift survey data and that the assumed spectral energy distributions are realistic. The observed far-infrared and submillimeter counts and background then provide strong constraints on the model parameters. The best fit for the $\Omega_0 = 1$ model is close to the star formation history predicted by the CDM scenario of Cole et al. (1994), but is significantly less peaked than the predictions of Pei & Fall (1995).

The models consistent with infrared and submillimeter counts and backgrounds tend to show a flat star formation rate from $z = 1$ to 3, consistent with the observed star formation history derived from HDF galaxies, using photometric redshifts and other UV, infrared, and submillimeter data (these will be discussed in a subsequent paper, Rowan-Robinson 2000). The most striking difference from previous modeling work is the dominant role predicted for the cirrus component at submillimeter wavelengths. This is a consequence of the requirement that all galaxies share a common star formation history. The models presented here are by no means unique. If a very strongly evolving, heavily obscured population of starbursts is postulated, as in the models of Franceschini et al. (1997, 1998) and Guiderdoni et al. (1998), then such a population will affect only the submillimeter counts and background (and perhaps the faintest 60 $\mu$m counts and redshift distributions). Existing 850 $\mu$m surveys (Hughes et al. 1998; Barger et al. 1998; Eales et al. 1999) suggest that at least some of the submillimeter galaxies may be luminous, opaque starbursts. The prediction here, however, is that most will show a cooler SED, and greater spatial extent, than expected for a typical M82- or Arp 220–like starburst.

Areas requiring further work are (1) the need to consider the evolution of the shape of the SEDs, particularly for the cirrus component, with redshift. The increased star formation rate at earlier times would tend to make the dust temperature higher, but this is partially offset by the much lower abundance of low-mass stars at earlier times. The evolution of the metallicity may also affect the grain properties and hence the SEDs (cf. Calzetti & Heckman 1999). (2) The AGN dust tori models require a further parameter, the orientation, and this may affect the AGN counts at optical wavelengths. (3) The tendency for the probability of finding an AGN component to increase with far-infrared luminosity is not fully reflected in the approach followed here. (4) It will be worthwhile to extend the predictions of these models to radio and X-ray wavelengths.

## APPENDIX

## COSMOLOGICAL FORMULAE

Collecting together the expressions for the cosmological observables, most of which are analytic functions, for the models consider here, we have for (model *a*) $\Lambda = 0$, the comoving radius

$$r(z) = \frac{2(1-\Omega_0)^{1/2}\{\Omega_0 z + (\Omega_0 - 2)[(1+\Omega_0 z)^{1/2} - 1]\}}{\Omega_0^2(1+z)},$$

the luminosity distance

$$D_{\rm lum}(z) = (1-\Omega_0)^{1/2}(1+z)r(z)(c/H_0),$$

the comoving volume

$$V(z) = 0.5\{r(1+r^2)^{1/2} + \ln[r + (1+r^2)^{1/2}]\}(c/H_0)^3,$$

and the age of the universe (in units of the Hubble time)

$$H_0\, t(z) = \frac{[(1-\Omega_0)(1+\Omega_0 z)]^{1/2}}{\Omega_0(1+z)} - 0.5\ln\frac{2-\Omega_0+\Omega_0 z + 2[(1-\Omega_0)(1+\Omega_0 z)]^{1/2}}{\Omega_0(1+z)},$$

$$H_0\, t_0 = \frac{(1-\Omega_0)^{1/2}}{\Omega_0} - 0.5\ln\frac{2-\Omega_0+2(1-\Omega_0)^{1/2}}{\Omega_0}.$$

For model *b*, $k = 0$, all the relations are analytic except that for $r(z)$, which is an elliptic integral and must be evaluated numerically. The comoving radius is

$$r(z) = 2(1-\Omega_0)^{1/2}\int_{\sqrt{(1/(1+z)}}^{1}\left[\frac{\Omega_0}{(1-\Omega_0)+y^6}\right]^{-1/2} dy,$$

the luminosity distance

$$D_{\rm lum}(z) = (1 + z)r(z)(c/H_0) ,$$

the comoving volume

$$V(z) = \frac{r^3(c/H_0)^3}{3} ,$$

and the age of the universe (in units of the Hubble time) is

$$H_0\, t(z) = 2 \sinh^{-1} \frac{[(1 - \Omega_0)/\Omega_0]^{1/2}(1 + z)^{-3/2}}{3(1 - \Omega_0)^{1/2}} ,$$

$$H_0\, t_0 = 2 \sinh^{-1} \frac{[(1 - \Omega_0)/\Omega_0]^{1/2}}{3(1 - \Omega_0)^{1/2}} .$$

## REFERENCES


Barger, A. J., Cowie, L. L., & Sanders, D. B. 1999, ApJ, 518, L5
Barger, A. J., Cowie, L. L., Sanders, D. B., Fulton, E., Taniguchi, Y., Sato, Y., Kawara, K., & Okuda, H. 1998, Nature, 394, 248
Baugh, C., Cole, S., Frenk, C., & Lacey, C. 1998, ApJ, 498, 504
Bertin, E., Dennefeld, M., & Moshir, M. 1997, A&A, 323, 685
Blain, A., Jameson, A., Smail, I., Longair, M. S., Kneib, J.-L., & Ivison, R. J. 1999a, MNRAS, 309, 715
Blain, A. W., Kneib, J.-P., Ivison, R. J., & Smail, I. 1999b, ApJ, 512, L87
Blain, A. W., & Longair, M. S. 1993, MNRAS, 264, 509
Blain, A. W., Smail, I., Ivison, R. J., & Kneib, J.-P. 1999c, MNRAS, 302, 632
Boyle, B. J., Shanks, T., & Peterson, B. A. 1988, MNRAS, 235, 935
Bruzual, A. G., & Charlot, S. 1993, ApJ, 405, 538
Calzetti, D., & Kinney, A. L. 1992, ApJ, 399, L39
Calzetti, F., & Heckman, T. M. 1999, ApJ, 519, 27
Cole, S., Aragon-Salamanca, A., Frenk, C. S., Navarro, J. F., & Zepf, S. E. 1994, MNRAS, 271, 781
Colless, M., Ellis, R. S., Broadhurst, T. J., Taylor, K., & Peterson, B. A. 1993, MNRAS, 261, 19
Condon, J. J. 1974, ApJ, 188, 279
Dickinson, M. 1998, in The Hubble Deep Field, ed. M. Livio, S. M. Fall, & P. Madau (Baltimore: STScI), 219
Dole, H., et al. 2000, in The Universe as Seen by *ISO*, ed. P. Cox & M. F. Kessler (ESA SP-427; Paris: ESA), 1031
Dunne, L., Eales, S., Edmunds, M., Ivison, R., Alexander, P., & Clements, D. L. 2000, MNRAS, 315, 115
Dwek, E., & Arendt, R. G. 1998, ApJ, 508, L9
Dwek, E., et al. 1998, ApJ, 508, 106
Eales, S., Lilly, S. J., Gear, W. K., Dunne, L., Bond, J. R., Hammer, F., Le Fevre, O., & Crampton, D. 1999, ApJ, 515, 518
Efstathiou, A., Rowan-Robinson, M., & Siebenmorgen, R. 2000, MNRAS, 313, 734
Elbaz, D., et al. 2000, A&A Lett., in press (preprint astro-ph/9910406)
Fixsen, D. J., Dwek, E., Mather, J. C., Bennett, C. L., & Shafer, R. A. 1998, ApJ, 508, 123
Flores, H., et al. 1999, ApJ, 517, 148
Fox, M. J. 2000, Ph.D. thesis, Univ. London
Franceschini, A., Mazzei, P., de Zotti, G., & Danese, L. 1994, ApJ, 427, 140
Franceschini, A., Silva, L., Fasano, G., Granato, G. L., Bressan, A., Arnouts, S., & Danese, L. 1998, ApJ, 506, 600
Franceschini, A., Toffolatti, L., Mazzei, P., Danese, L., & De Zotti, G. 1991, A&AS, 89, 285
Franceschini, A., et al. 1997, in The Far Infrared and Submillimeter Universe, ed. A. Wilson (ESA SP-401; Noordwijk: ESA), 159
Gispert, R., Lagache, G., & Puget, J.-L. 2000, A&A, 360, 1
Gorjian, V., Wright, E. L., & Chang, R. R. 2000, ApJ, 536, 550
Gregorich, D. T., Neugebauer, G., Soifer, B. T., Gunn, J. E., & Herter, T. L. 1995, AJ, 110, 259
Guiderdoni, B., Bouchet, F. R., Puget, J.-L., Lagache, G., & Hivon, E. 1997, Nature, 390, 257
Guiderdoni, B., Hivon, E., Bouchet, F. R., & Maffei, B. 1998, MNRAS, 295, 877
Hacking, P. B., & Houck, J. 1987, ApJS, 63, 311
Hauser, M. G., et al. 1998, ApJ, 508, 25
Hughes, D. H., et al. 1998, Nature, 394, 241
Kauffmann, G., & Haehnelt, M. 2000, MNRAS, 311, 576
Kauffmann, G., White, S. D. M., & Guiderdoni, B. 1993, MNRAS, 264, 201
Kawara, K., et al. 1998, A&A, 336, L9
Lagache, G., Abergel, A., Boulanger, F., Desert, F.-X., & Puget, J.-L. 1999, A&A, 344, 322
Lanzetta, K. M., Yahil, A., & Fernandez-Soto, A. 1996, Nature, 381, 759
Lilly, S. J., Le Fevre, O., Hammer, F., & Crampton, D. 1996, ApJ, 460, L1
Lilley, S. J., Tresse, L., Hammer, F., Crampton, D., & Le Fevre, O. 1995, ApJ, 455, 108
Lonsdale, C. J., Hacking, P. B., Conrow, T. P., & Rowan-Robinson, M. 1990, ApJ, 358, 60
Loveday, J., et al. 1992, ApJ, 390, 338
Madau, P., Ferguson, H. C., Dickinson, M. E., Giavalisco, M., Steidel, C. C., & Fruchter, A. 1996, MNRAS, 283, 1388
Madau, P., Pozzetti, L., & Dickinson, M. 1998, ApJ, 498, 106
McCracken, H. J., Metcalfe, N., Shanks, T., Campos, A., Gardner, J. P., & Fong, R. 2000, MNRAS, 311, 707
Metcalfe, N., Shanks, T., Fong, R., & Roche, N. 1995, MNRAS, 273, 257
Meurer, G. R., Heckman, T. M., & Calzetti, D. 1999, ApJ, 521, 64
Meurer, G. R., Heckman, T. M., Lehnert, M. D., Leitherer, C., & Lowenthal, J. 1997, AJ, 114, 54
Murdoch, H. S., Crawford, D. F., & Jauncey, D. L. 1973, ApJ, 183, 1
Oliver, S. J., et al. 1996, MNRAS, 280, 673
———. 1997, MNRAS, 289, 471
Pearson, C., & Rowan-Robinson, M. 1996, MNRAS, 283, 174
Pei, Y. C., & Fall, S. M. 1995, ApJ, 454, 69
Pettini, M., Kellogg, M., Steidel, C. C., Dickinson, M., Adelberger, K. L., & Giavalisco, M. 1998, ApJ, 508, 539
Pozzetti, L., Madau, P., Ferguson, H. C., Zamorani, G., & Bruzual, G. A. 1998, MNRAS, 298, 1133
Puget, J.-L., Abergal, A., Bernard, J.-P., Boulanger, F., Burton, W. B., Desert, F.-X., & Hartmann, D. 1966, A&A, 308, 5
Rigopoulou, D., Lawrence, A., & Rowan-Robinson, M. 1996, MNRAS, 278, 1049
Rowan-Robinson, M. 1995, MNRAS, 272, 737
———. 1999a, in ASP Conf. Ser. 177, Astrophyics with Infrared Surveys: A Prelude to SIRTF, ed. M. D. Bicay et al. (San Francisco: ASP), 127
———. 1999b, Ap&SS, 266, 291
———. 2000, ApJ, submitted
Rowan-Robinson, M., & Crawford, J. 1989, MNRAS, 238, 523
Rowan-Robinson, M., & Efstathiou, A. 1993, MNRAS, 263, 675
Rowan-Robinson, M., Larence, A., & Saunders, W. 1991, MNRAS, 253, 485
Rowan-Robinson, M., et al. 1997, MNRAS, 289, 490
Rush, B., Malkan, M. A., & Spinoglio, L. 1993, ApJS, 89, 1
Saunders, W., Rowan-Robinson, M., Lawrence, A., Efstathiou, G., Kaiser, N., & Frenk, C. S. 1990, MNRAS, 242, 318
Saunders, W., et al. 2000, MNRAS, 317, 55
Schlegel, D. J., Finkbeiner, D. P., & Davis, M. 1998, ApJ, 500, 525
Serjeant, S., et al. 2000, MNRAS, 316, 768
Smail, I., Ivison, R. J., & Blain, A. W. 1997, ApJ, 490, L5
Somerville, R. S., Primack, J. R., & Faber, S. M. 2000, MNRAS, 320, 504
Steidel, C. C., Adelberger, K. L., Giavalisco, M., Dickinson, M., & Pettini, M. 1999, ApJ, 519, 1
Verma, A. 2000, Ph.D. thesis, Univ. London
Walker, T. P., Steigman, G., Schramm, D. N., Olive, K. A., & Kang, H.-S. 1991, ApJ, 376, 51
Wright, E. L., & Reese, E. D. 2000, ApJ, 545, 43
Xu, C., Hacking, P. B., Fang, F., Shupe, D. L., Lonsdale, C. J., Lu, N. Y., Helou, G., Stacey, G. J., & Ashby, M. L. N. 1998, ApJ, 508, 576
Yoshii, Y., & Takahara, F. 1988, ApJ, 326, 1